Supporting Information

Unveil the Effect of Water on Photoinduced Electron Transfer by Crystallographic Study

Peng-Hao Wang,[a] Xiao-Yue Zhang,[a] Jin-Ai Fan[a] and Cai Sun*[ab]

[a]College of Chemistry, Fuzhou University, Fuzhou, Fujian 350108, China

[b]State Key Laboratory of Structural Chemistry, Fujian Institute of Research on the Structure of Matter, Chinese Academy of Sciences, Fuzhou, Fujian 350002, China

E–mails: csun@fzu.edu.cn (C. Sun)

Index:

1. Experimental section

Materials and measurements. All commercially available chemicals were of analytical reagent grade and used as received without further purification. Water was deionized and distilled before use. Elemental analyses of C, H, and N were measured on an Vario MICRO CHNOS Elementar Analyzer. FT-IR spectra were measured on a PerkinElmer Spectrum One FT-IR spectrometer using KBr pellets. Solid state UV–vis absorption spectra were measured in the absorption mode on PerkinElmer Lambda 900 UV/vis/near-IR spectrophotometer equipped with an integrating sphere, and a $BaSO_4$ plate was used as the reference. PXRD patterns were recorded using Cu-$K\alpha$ radiation on a Rigaku Desktop MiniFlex 600 diffractometer powered at 30 kV and 15 mA. Thermogravimetric analyses (TGA) were performed on a Mettler TOLECO TGA apparatus with a heating rate of 10 °C/min in nitrogen atmosphere. Electron paramagnetic resonance (EPR) spectra were recorded on a Bruker ER-420 spectrometer with a 100 kHz magnetic field in the X band at room temperature.

Synthesis of 2,4,6-trinitrophenol. Phenol (540 mg, 5.3 mmol) was dissolved in 1 mL of DMSO in a 50 mL round-bottomed flask and then 4 mL of 63% nitric acid was slowly dropwise added to the solution in the ice-water bath. A large amount of gas is produced in the round-bottomed flask during the drip process and the mixture became brown. After gentle stirring, the mixture was heated under reflux for 5 h. The reaction evolved a deep brown gas and the mixture changed color from brown to yellow at the end. The final reaction mixture was cooled in an ice-water bath and diluted with 30 mL of ice-water. The precipitated solid was filtered off, washed with ice-water, and finally dried at room temperature to yield pale-yellow crystals, 765 mg (62.8% yield).

Synthesis of 1. 2,4,6-trinitrophenol (115 mg, 0.5 mmol) and 4,4'-Bipyridine (bpy) (37 mg, 0.25 mmol) are dissolved separately in the mixed solution of water/ethanol (4:1). The two solutions mix with each other to form a yellow precipitate of **1**. And the product was filtered to yield a bright yellow clear liquid, which was allowed to volatilize in the dark for 3 d to obtain the crystals of **1**. The all yield of **1** based on bpy is 87.4%. Elemental analysis: Found: C, 40.93, H, 2.43, N, 17.38%; Calc for **1**: C, 40.58, H, 2.76, N, 17.21%.

Synthesis of 2. 2,4,6-trinitrophenol (115 mg, 0.5 mmol) and 4,4'-Bipyridine (bpy) (37 mg, 0.25 mmol) are dissolved separately in the mixed solution of water/ethanol (1:4). The two solutions mix with each other to form a yellow precipitate of **2**. And the product was filtered to yield a bright yellow clear liquid, which was allowed to volatilize in the dark for 3 d to obtain the crystals of **2**. The all yield of **2** based on bpy is 90.8%. Elemental analysis: Found: C, 41.89, H, 2.22, N, 17.76%; Calc for **2**: C, 41.74, H, 2.52, N, 17.7%.

Synthesis of 3. 2,4,6-trinitrophenol (115 mg, 0.5 mmol) and 4,4'-Bipyridine (bpy) (37 mg, 0.25 mmol) are dissolved separately in the mixed solution of ethanol. The two solutions mix with each other to form a yellow precipitate of **3**. And the product was filtered to yield a bright yellow clear liquid, which was allowed to volatilize in the dark for 3 d to obtain the crystals of **3**. The all yield of **3** based on bpy is 94.7%. Elemental analysis: Found: C, 43.08, H, 2.04, N, 18.4%; Calc for **3**: C, 42.96, H, 2.27, N, 18.22%.

X-ray crystallographic study. Suitable single crystal of compound **3** was carefully selected and performed. Intensity data for single crystal was collected on a ROD, Rigaku SATURN70 CCD diffractometer with graphite-monochromatized Mo $K\alpha$ radiation (λ = 0.71073 Å). A multi-scan absorption correction was performed using CrysAlisPro 1.171.40.59a (Rigaku Oxford Diffraction, 2019) Empirical absorption correction using spherical harmonics, implemented in SCALE3 ABSPACK scaling algorithm. The structure was solved and refined on F^2 by full-matrix least squares technique using the SHELX-2019 program package and by using Olex2 1.5-dev as the graphical interface. All non-hydrogen atoms were refined anisotropically. Hydrogen atom positions were calculated geometrically and refined using the riding model. Most hydrogen atom positions were calculated geometrically and refined using the riding model, but some hydrogen atoms were

refined freely. Crystal data and structure refinement results for **3** summarized in **Table S1**. The authors sincerely thank the reviewer for the refinement of the position of H atoms.

The entries of CCDC-2202211, contain the supplementary crystallographic data for **3**, respectively. These data can be obtained free of charge at http://www.ccdc.cam.ac.uk/conts/retrieving.html or from the Cambridge Crystallographic Data Centre, 12, Uni on Road, Cambridge CB2 1EZ, U.K. Fax: (Internet) +44-1223/336-033. E-mail: depos-it@ccdc.cam.ac.uk.

Computational approaches.

The structures of **1** and **2** were obtained from CCDC database. The crystal structure of **1**–**3** were applied to build calculation models. Because the positions of H atoms are difficult to be accurately determined by the method of single crystal X-ray diffraction, the geometry optimizations of **1**–**3**, where the position of H atoms were optimized and other atoms were freezing, were performed with PBE/6-31g* level in the CP2K software.[1] The molecular orbitals were calculated at same level (Fig. 1 d–f). Subsequent computational models and structural diagrams in the manuscript (Fig. 1 a–c) were based on the optimized structures (see atomic coordinate in file of 1_optH.cif, 2_optH.cif, and 3_optH.cif for **1**, **2** and **3**, respectively). A density-fitted SAPT calculations (Fig. 3, Table S4) were performed at the SAPT0 level using the SAPT module in the PSI4 software package.[2] A truncated aug-cc-pVDZ basis (i.e. jun-cc-pVDZ) was used, which was optimal with the SAPT0 level due to the good performance in error cancellation.[3] The frozen core approximation with the default setting was also used. The calculations of electrostatic potential (Fig. 4) were implemented at the ORCA software with B3LYP-D3(BJ)/def2-TZVP(-f) level.[4] The input files were generated with help of Multiwfn program.[5]

2. Supplementary data

1) Crystal and structure refinement data

Table S1. Crystal and structure refinement data for **3**.

	3
Formula	$C_{22}H_{18}N_8O_{16}$
Mr	650.43
Crystal size (*mm³*)	0.30 × 0.20 × 0.08
Crystal system	monoclinic
Space group	*C*2/c
a (Å)	13.9035 (10)
b (Å)	15.8033 (8)
c (Å)	119884 (8)
α (deg)	90
β (deg)	100.747 (6)
γ (deg)	90
V (Å³)	2587.7 (3)
D_{calcd} (g/cm³)	1.670
Z	4
F(000)	1337.3
Abs coeff (mm⁻¹)	0.145
Reflns collcd/unique (R_{int})	10133/2649 (0.0336)
Data/params/restraints	1963/219/0
$R_1{}^a$	0.0458
$\omega R_2{}^b$	0.1248
GOF on F^2	1.0314
$\Delta\rho_{max}$ and $\Delta\rho_{min}$(e/Å⁻³)	0.2174 and -0.3146

$^a R_1 = \Sigma||F_o|-|F_c||/\Sigma|F_o|$, $^b \omega R_2 = \{\Sigma\omega[(F_o)^2-(F_c)^2]^2/\Sigma\omega[(F_o)_2]^2\}^{1/2}$

Table S2 Interaction components (kcal/mol) between H_2V and tnp in **1**, **2** and **3**, calculated at the SAPT level.

	Dispersion	Electrostatics	Induction	Exchange	Total sSAPT0
1	-7.406	-126.492	-28.218	21.860	-140.257
2	-6.576	-120.990	-26.724	20.118	-134.172
3	-2.235	-90.792	-8.151	3.359	-97.820

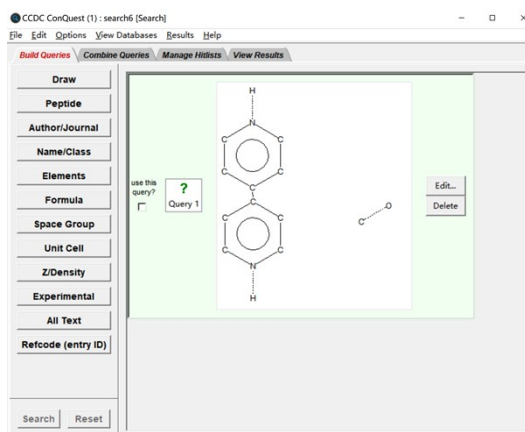**2) Screening condition and result.**

Figure S1. Screening conditions, including 'H$_2$V', and 'C–O' groups, for potential donor-acceptor system with different equivalent water molecules.
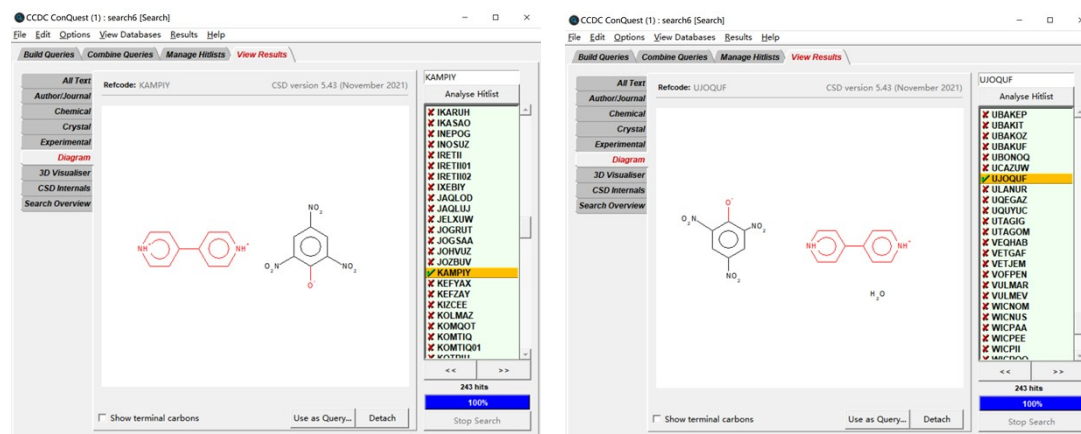

Figure S2. The 243 hits, that are, H$_2$V(tnp)$_2$ (**1**) and H$_2$V(tnp)$_2$·H$_2$O (**2**), were selected considering its well-resolved crystal structure, same donor-acceptor system with different equivalent water molecules, and potential electron-transfer photochromic property.
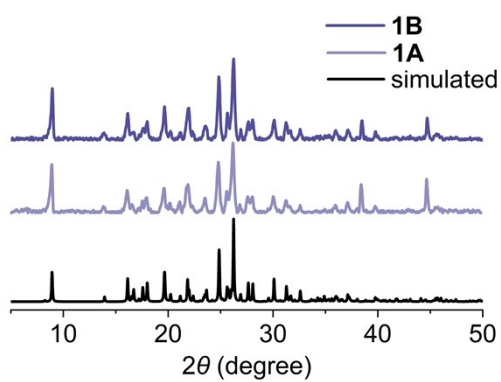
3) PXRD patterns

Figure S3. Experimental and simulated PXRD patterns of **1**.
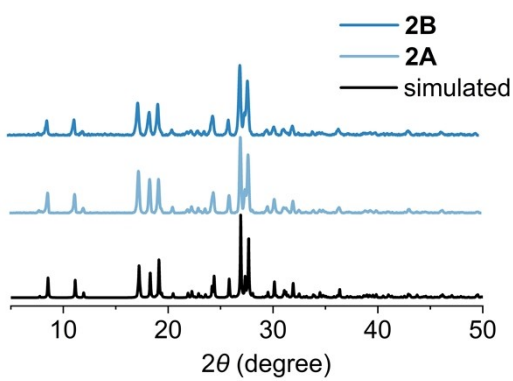
Figure S4. Experimental and simulated PXRD patterns of **2**.
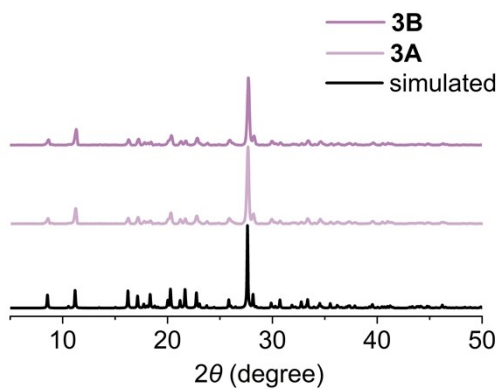
Figure S5. Experimental and simulated PXRD patterns of **3**.
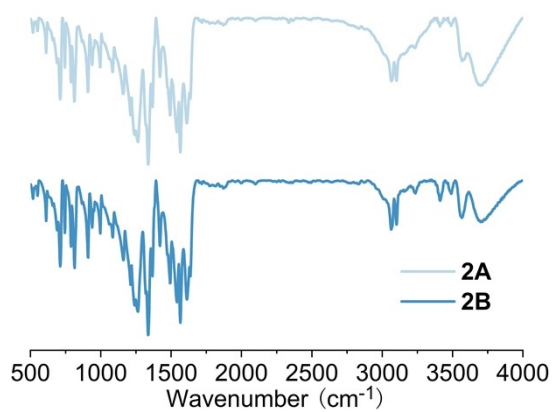
4) IR spectra
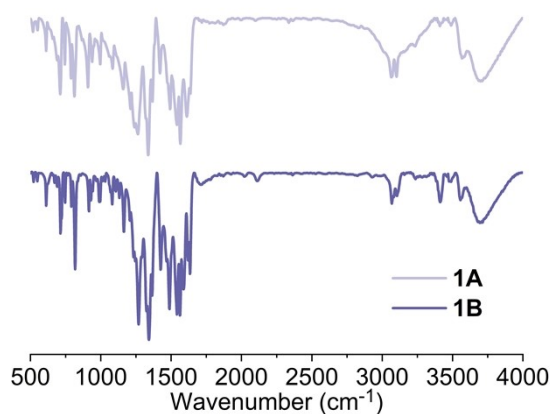
Figure S6. FT-IR spectra of the as-synthesized (**1A**) and colored (**1B**) samples.

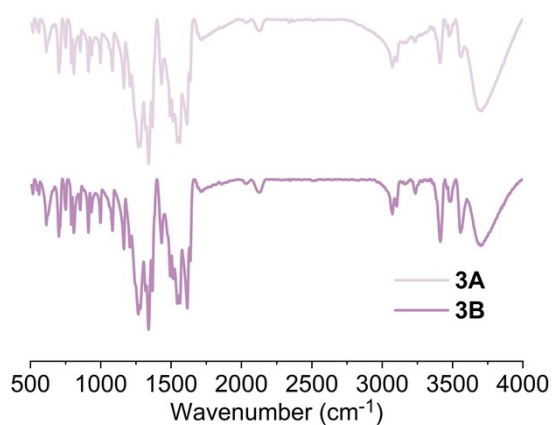**Figure S7** FT-IR spectra of the as-synthesized (**2A**) and colored (**2B**) samples.

Figure S8. FT-IR spectra of the as-synthesized (**3A**) and colored (**3B**) samples.
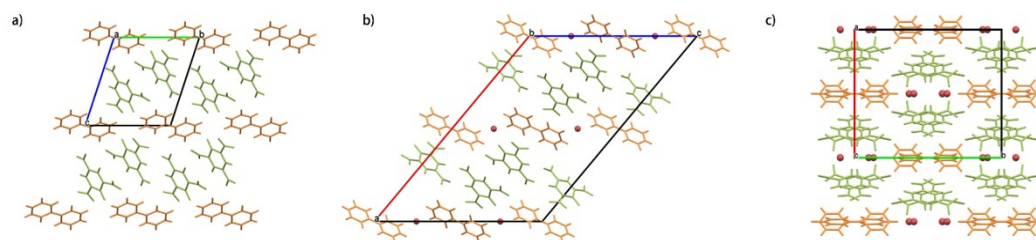
5) Crystal packing

Fig. S9 Crystal packing of **1** (a), **2** (b) and **3** (c). H_2V and tnp are coloured in orange and green, respectively. The disorder of hydrogen in water has been removed for clarity. Compound **1** crystallized in the triclinic crystal system (space group $P\bar{1}$) with Z = 1. Compound **2** and **3** both crystallized in the same monoclinic crystal system (space group $C2/c$) with Z = 4. The phenolic protons of trinitrophenol were transferred to the 4,4'-bipyridine in these compounds through Bronsted acid-base interactions, resulting H_2V cation and two tnp anions. Interestingly, the H_2V dications and tnp anions in these compounds were all arranged alternately in layers to form the pillared structure. One equivalent water molecule and two equivalent water molecules exist in the H_2V layer for **2** and **3**, respectively.
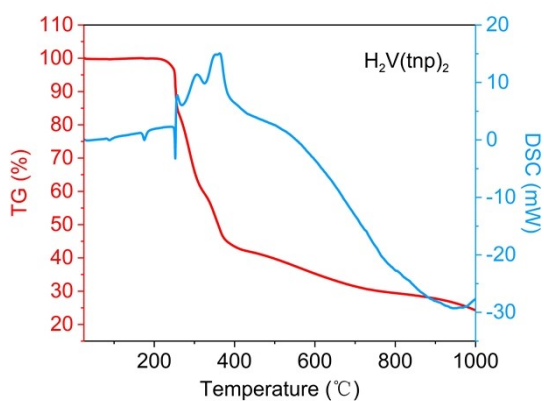
6) Thermogravimetric analysis

Figure S10. Thermogravimetric analysis of **1** in nitrogen atmosphere with the ramp rate of 10 °C/min.

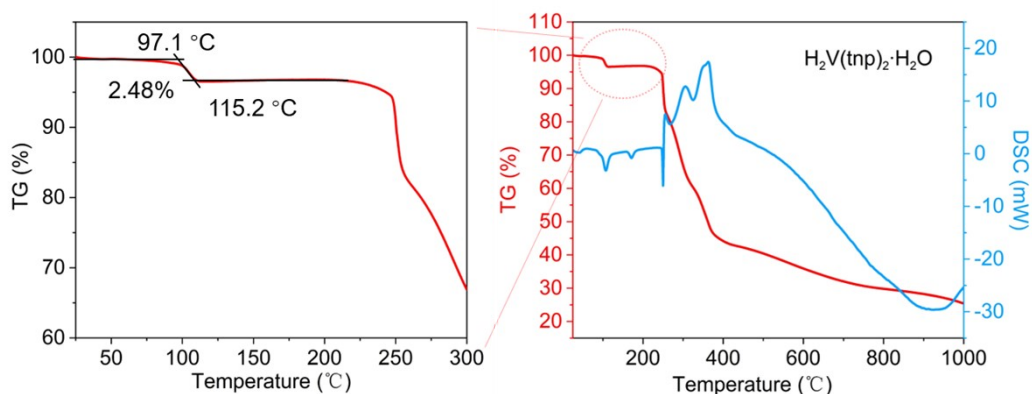**Figure S11.** Thermogravimetric analysis of **2** in nitrogen atmosphere with the ramp rate of 10 °C/min (right) and enlarged TG curve ranging from RT to 300 °C (left). Water molecules analysis: Found: 2.48%; Calc: 2.84%.

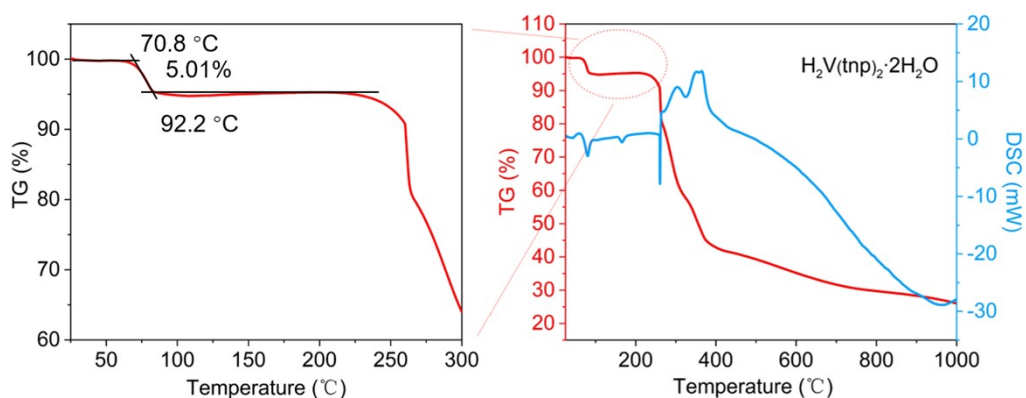**Figure S12.** Thermogravimetric analysis of **3** in nitrogen atmosphere with the ramp rate of 10 °C/min (right) and enlarged TG curve ranging from RT to 300 °C (left). Water molecules analysis: Found: 5.01%; Calc: 5.53%.

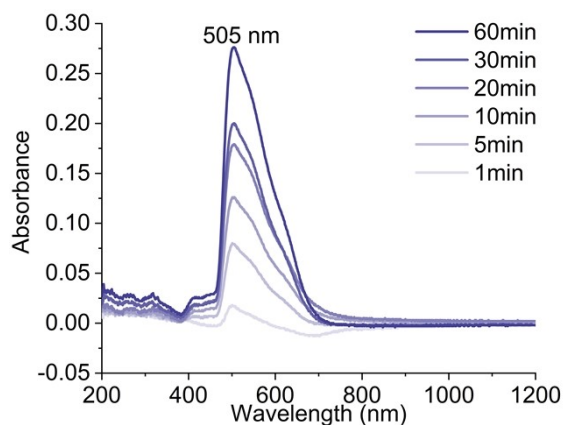**7) The difference value of time-dependent photochromic process**

Figure S13. The difference value of time-dependent electron absorption spectra upon irradiation for **1**.
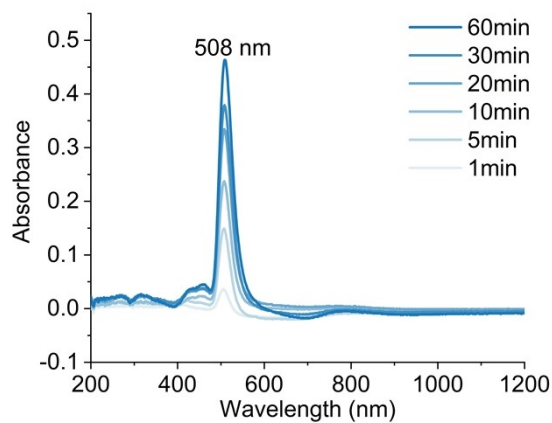

Figure S14. The difference value of time-dependent electron absorption spectra upon irradiation for **2**.
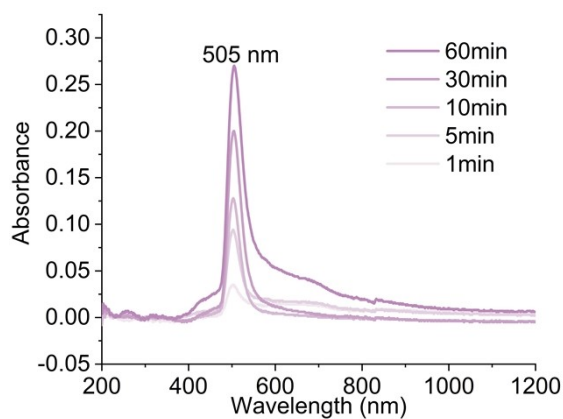

Figure S15. The difference value of time-dependent electron absorption spectra upon irradiation for **3**.

3. References

1. T. D. Kuehne, M. Iannuzzi, M. Del Ben, V. V. Rybkin, P. Seewald, F. Stein, T. Laino, R. Z. Khaliullin, O. Schutt, F. Schiffmann, D. Golze, J. Wilhelm, S. Chulkov, M. H. Bani-Hashemian, V. Weber, U. Borstnik, M. Taillefumier, A. S. Jakobovits, A. Lazzaro, H. Pabst, T. Mueller, R. Schade, M. Guidon, S. Andermatt, N. Holmberg, G. K. Schenter, A. Hehn, A. Bussy, F. Belleflamme, G. Tabacchi, A. Gloss, M. Lass, I. Bethune, C. J. Mundy, C. Plessl, M. Watkins, J. VandeVondele, M. Krack and J. Hutter, *J. Chem. Phys.*, 2020, **152**, 194103.

2. D. G. A. Smith, L. A. Burns, A. C. Simmonett, R. M. Parrish, M. C. Schieber, R. Galvelis, P. Kraus, H. Kruse, R. Di Remigio, A. Alenaizan, A. M. James, S. Lehtola, J. P. Misiewicz, M. Scheurer, R. A. Shaw, J. B. Schriber, Y. Xie, Z. L. Glick, D. A. Sirianni, J. S. O'Brien, J. M. Waldrop, A. Kumar, E. G. Hohenstein, B. P. Pritchard, B. R. Brooks, H. F. Schaefer, III, A. Y. Sokolov, K. Patkowski, A. E. DePrince, III, U. Bozkaya, R. A. King, F. A. Evangelista, J. M. Turney, T. D. Crawford and C. D. Sherrill, *J. Chem. Phys.*, 2020, **152**, 184108.

3. T. M. Parker, L. A. Burns, R. M. Parrish, A. G. Ryno and C. D. Sherrill, *J. Chem. Phys.*, 2014, **140**, 094106.

4. F. Neese, *Wiley Interdisciplinary Reviews-Computational Molecular Science*, 2018, **8**, e1327.

5. T. Lu and F. Chen, *J. Comput. Chem.*, 2012, **33**, 580-592.